

Iterative Synthesis of Contorted Macromolecular Ladders for Fast-Charging and Long-Life Lithium Batteries

Zexin Jin,^{*,§} Qian Cheng,[§] Si Tong Bao, Ruiwen Zhang, Austin M. Evans, Fay Ng, Yunyao Xu, Michael L. Steigerwald, Ann E. McDermott, Yuan Yang,^{*} and Colin Nuckolls^{*}



Cite This: <https://doi.org/10.1021/jacs.2c06527>



Read Online

ACCESS |



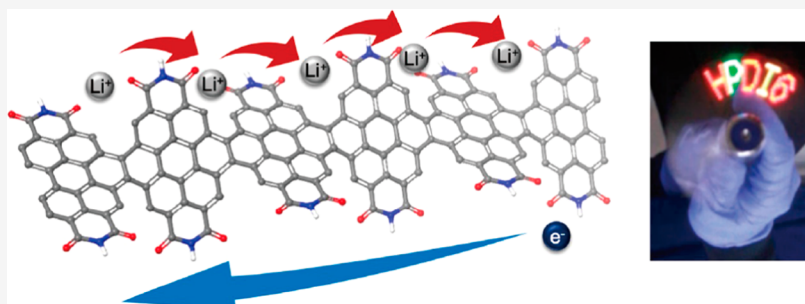
Metrics & More



Article Recommendations



Supporting Information



ABSTRACT: We report here an iterative synthesis of long helical perylene diimide (**hPDI**[*n*]) nanoribbons with a length up to 16 fused benzene rings. These contorted, ladder-type conjugated, and atomically precise nanoribbons show great potential as organic fast-charging and long-lifetime battery cathodes. By tuning the length of the **hPDI**[*n*] oligomers, we can simultaneously modulate the electrical conductivity and ionic diffusivity of the material. The length of the ladders adjusts both the conjugation for electron transport and the contortion for lithium-ion transport. The longest oligomer, **hPDI**[6], when fabricated as the cathode in lithium batteries, features both high electrical conductivity and high ionic diffusivity. This electrode material exhibits a high power density and can be charged in less than 1 min to 66% of its maximum capacity. Remarkably, this material also has exceptional cycling stability and can operate for up to 10,000 charging–discharging cycles without any appreciable capacity decay. The design principles described here chart a clear path for organic battery electrodes that are sustainable, fast-charging, and long lasting.

INTRODUCTION

Lithium-ion batteries (LIBs)^{1–3} are the world's predominant energy storage devices and as such have significantly accelerated the development of today's digital information society.^{4–6} While current LIBs boast amazing performance, their power density and cycling stability are areas in need of improvement.^{7–12} This need is particularly acute for many applications, such as electric vehicles, due to the relatively long charging time and cycling capacity loss associated with current battery technologies.⁸ Compared to the current inorganic electrode materials, organic electrode materials (OEMs) provide unique opportunities to achieve high power density through molecular engineering that can, in principle, yield simultaneously high ionic diffusivity and high specific capacities.^{13–18} Further, OEMs benefit from being sustainable and “green” due to the earth abundance of their components, low cost to produce, and low environmental impact.^{19–21} However, one of the major issues regarding OEMs is their trade-off between specific capacity and cycling stability.¹⁷ Organic molecules, albeit with high capacity, leach into the electrolyte solution during the redox reactions, which results in poor cycling stability. Organic polymers can overcome the dissolution issue, but they typically have low charge capacity due

to the redox-inactive nature of their linkers and solubilizing side chains. Beyond these challenges, the low intrinsic electrical conductivity of OEMs has thwarted their ability to achieve high rate capability and high areal mass-loading.¹⁶ Consequently, incorporating a high ratio of conductive additives is usually necessary in electrode fabrication for organics to achieve idealized results, which further limits OEMs' technological utility.^{16,18}

Here, we describe a molecular design of contorted, fully conjugated, atomically precise, electroactive molecular ladders that simultaneously solves the fundamental issues associated with the existing classes of OEMs. These conjugated molecular ladders shown in Figure 1a, known as the helical perylene diimide (**hPDI**[*n*]), are significant because they have proven useful in photovoltaics,²² photosensors,²³ field-effect transistors,^{24,25} and as the electron transport layer in perovskite solar cells.^{25,26} Despite their good performance and excellent characteristics, the synthesis of the **hPDI**[*n*] series is not effective to synthesize ribbons that are longer than four PDI

Received: June 21, 2022

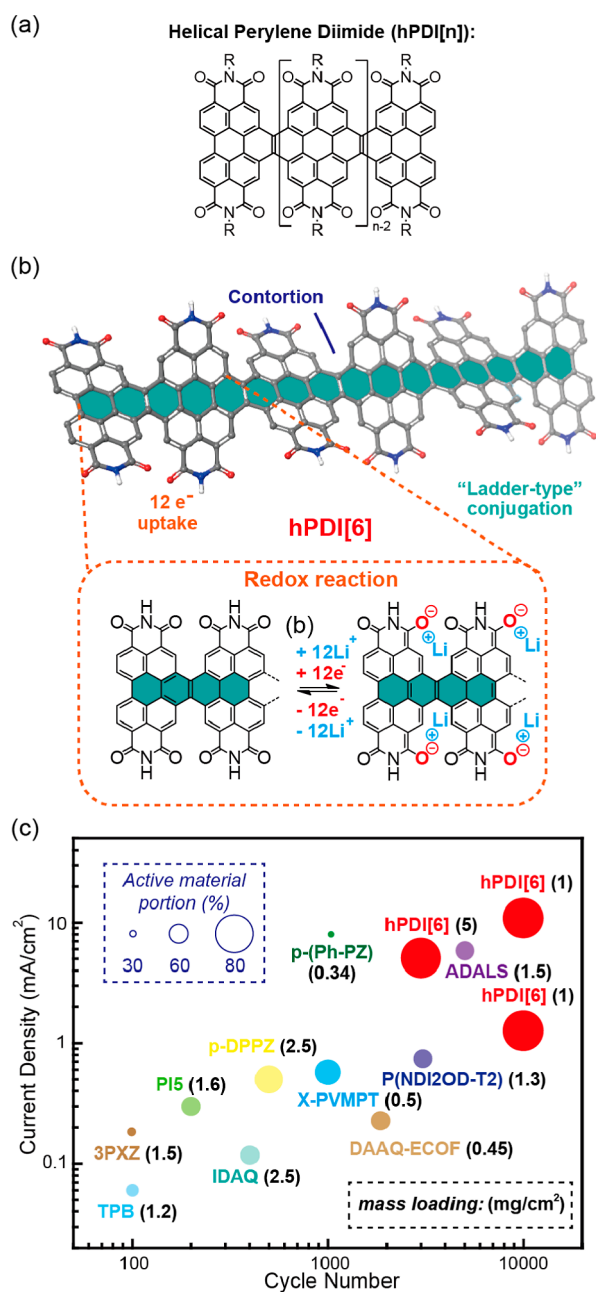


Figure 1. (a) Helical perylene diimide nanoribbons. (b) Schematics of hPDI[6] as a fast-charging lithium battery cathode. (c) Performance comparison of hPDI[6] with other reported OEMs with similar mass loadings and specific capacities (100–250 mAh/g). The active material portions are indicated by the size of the circles, and the average active material mass loadings are shown in parentheses. The three red circles for hPDI[6] represent three different cells cycled at different currents or mass loadings. See Table S1 (Supporting Information) for detailed information used in this graph.

subunits (i.e., hPDI[4]).²⁴ This paper describes a new synthetic method that allows them to be synthesized in a longer form with up to 16 fused benzene rings (hPDI[6], Figure 1b), allowing us to study the optoelectronic properties of the family. Furthermore, we demonstrated these molecular ladders have great potential as fast-charging and long-life OEMs. The most efficacious member of this series, hPDI[6], highlights four design principles for organic electrodes to achieve exceptional rate capability and cycling stability (Figure 1b): (1) redox-active

PDI subunits that feature high stability and fast redox kinetics;^{27,28} (2) insoluble macromolecules that overcome the dissolution issue associated with small molecules; (3) molecular contortion that facilitates lithium-ion transport and thus leads to high ionic diffusivity within the solid material;²⁹ and (4) a precisely defined fully conjugated ladder structure that provides high electrical conductivity.

When hPDI[6] is formulated as a cathode, it shows excellent rate performance of 126 and 87 mAh/g (96 and 66% retention of its theoretical capacity) under current densities of 1 A/g (7.7 C) and 10 A/g (77 C), respectively. Such a high rate performance significantly reduces the charging time to less than 1 min and leads to an output power density of up to 22,500 W/kg. Moreover, hPDI[6] cathodes exhibit exceptional cycling stability up to over 10,000 charge–discharge cycles with capacity fades of 0.004 and 0.0017% per cycle for 7.7 and 77 C, respectively. Importantly, these hPDI[6] cathodes are fabricated with a high active material portion of 80 wt %, which is unusually high for organic electrodes.¹⁸ Figure 1c shows the particular advantages of this design over state-of-the-art organic cathodes by its rate performance, cycling stability, and active material portion. To demonstrate the practical relevance, we assembled coin cells with high active mass loading (5 mg/cm², shown in Figure 1c) and with high temperature (60 °C) operation capability and pouch cells that are able to power a commercial LED fan. This new material and the associated design strategy set forth a path for sustainable, fast-charging, and long-lifetime organic batteries.

RESULTS AND DISCUSSION

Iterative Synthesis of hPDI[n]. PDI-based molecules and polymers have been investigated as electrode materials by other research groups because of its stable redox reaction. However, due to a densely packed structure and low electrical conductivity,³⁰ the materials showed limited power density and poor cycling stability (Table S2). We hypothesized that the electrical conductivity and ionic diffusion could be simultaneously improved by increasing both the length of π -conjugation and the number of contorted aromatic sites. In addition, a longer fully conjugated system can stabilize the reduced states, thus making the redox-active groups more accessible (Figure 1b). Critical to this study was the need to synthesize atomically defined, ladder-type fully conjugated structures of substantial length. However, previous synthetic approaches²⁴ that used to synthesize hPDI[n] (up to $n = 4$) do not allow the production of longer ribbons due to incomplete photocyclization.

Two observations guided our synthetic plan for the preparation of longer oligomers. First, in our prior synthesis of hPDI[4], we found that the photocyclization of the precursor with an internal double bond flanked by two hPDI[2] precursors results in recovery of the starting material and essentially no photocyclization.²⁴ Second, previous reports³¹ indicate that the photocyclization on PDI to form benzo-PDI (formation of the A-bond shown in Figure 2a) is much more facile than the photocyclization to the coronenediimide (formation of the B-bond shown in Figure 2a). Putting these two factors together, we hypothesized that the formation of “Type B” precursors shown in Figure 2b would lead to an efficient and high yielding synthesis of hPDI[5]-C11 and hPDI[6]-C11 (C11 refers to the branched undecyl-solubilizing groups).

Scheme 1 displays the iterative synthesis of hPDI[5]-C11 and hPDI[6]-C11 from shorter ribbons of hPDI[3]-C11 and

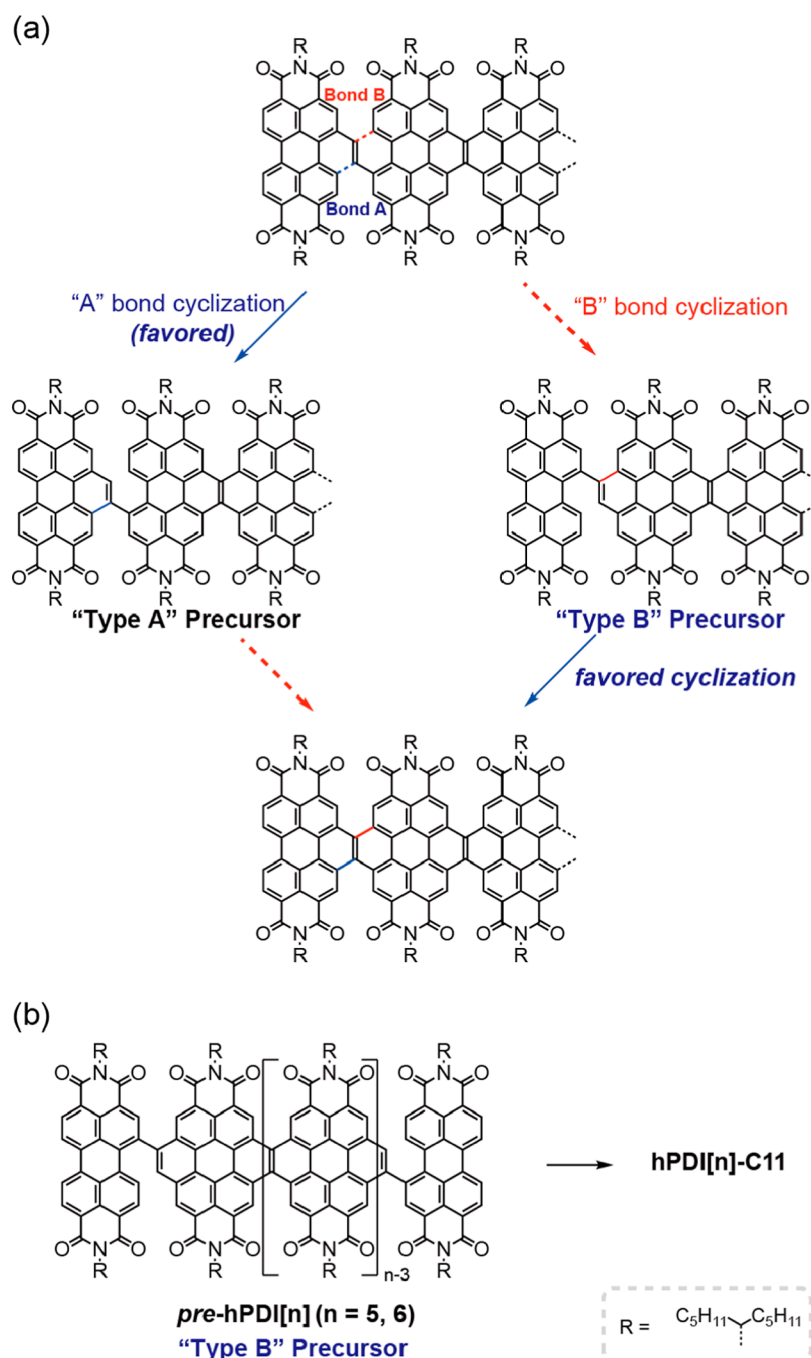
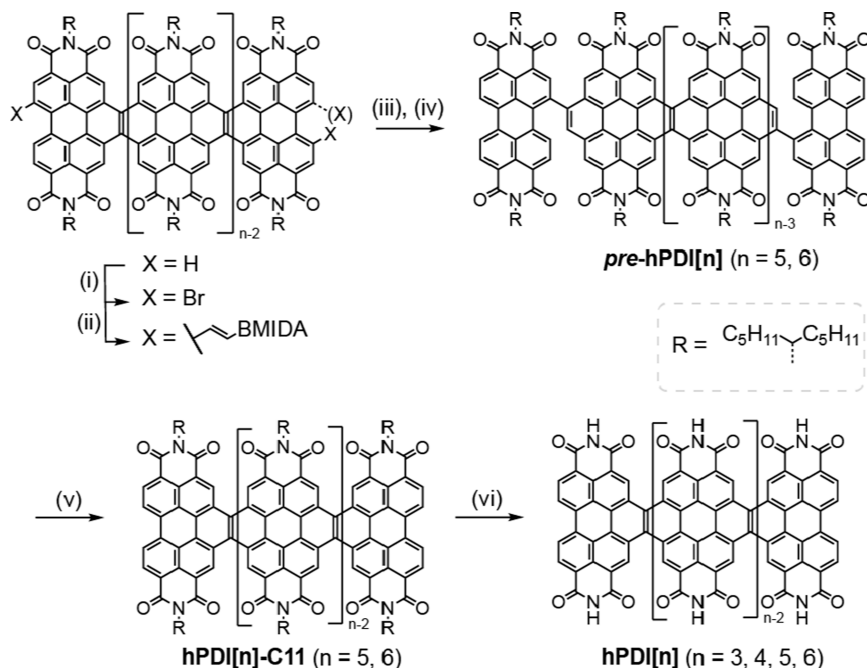


Figure 2. (a) Cyclization sequence of **hPDI[n]** precursors. (b) Hypothesized precursors for longer **hPDI[n]** ribbons.

hPDI[4]-C11, respectively. We first dibrominated **hPDI[3]-C11** using a large excess of bromine in dichloromethane at room temperature. Since MIDA boronates can serve as masked boronic acid reagents,^{31–33} we installed an ethylene *N*-methyliminodiacetate (MIDA) boronate group on **hPDI[3]** by Suzuki coupling with a *trans*-2-(pinacol boronate)-vinylboronic acid MIDA ester. We then subjected **DiBmida-hPDI[3]** to Mallory photocyclization using iodine and light under room temperature. We deprotected the MIDA boronates and reacted this with PDI-Br to give the "Type B" precursor **pre-hPDI[5]**. To complete the synthesis of **hPDI[5]-C11**, we irradiated **pre-hPDI[5]** with a common visible light LED in the presence of iodine in chlorobenzene at 90 °C. **hPDI[5]** formed quantitatively in 2 h. We purified the product by simply removing

the solvent and washing with methanol. Using this same approach, we synthesized **hPDI[6]-C11** from **hPDI[4]-C11**. Importantly, this new procedure is applicable to longer and functionalized **hPDI[n]** nanoribbons. We then performed vacuum thermolysis on **hPDI[n]-C11** at 360 °C to quantitatively remove the alkyl chains (see thermogravimetric analysis, [Figure S1](#)). The resulting **hPDI[n]** exhibited enhanced gravimetric capacity by reducing the electro-inactive mass, simultaneously rendering the material insoluble ([Figure S28](#)). **hPDI[2]** was not included due to the unsuccessful thermolysis from corresponding **hPDI[2]-C11**. The structure of **hPDI[n]** ($n = 3–6$) was confirmed by ¹³C solid-state NMR, infrared spectroscopy, and MALDI mass spectrometry (characterization

Scheme 1. Synthesis of hPDI[5]-C11, hPDI6-C11, and hPDI[n] ($n = 3-6$)^a

^aReaction conditions: (i) Br_2 , CH_2Cl_2 , rt. (ii) *trans*-2-(pinacol boronate)vinylboronic acid MIDA ester, $\text{Pd}(\text{dppf})\text{Cl}_2$, K_3PO_4 , $\text{THF}/\text{H}_2\text{O}$, rt. (iii) I_2 , DCM , $h\nu$, rt. (iv) PDI-Br , $\text{Pd}(\text{dppf})\text{Cl}_2$, K_2CO_3 , $\text{THF}/\text{H}_2\text{O}$, 57°C . (v) I_2 , PhCl , $h\nu$, 90°C . (vi) 360°C , in vacuum. MIDA: *N*-Methyliminodiacetate.

and synthetic details can be found in Supporting Information, sections 2 and 3).

Electrical Conductivity and Effective Conjugation Length of hPDI[n]. We measured the electrical conductivity of the hPDI[n] ($n = 3-6$) thin films using a two-probe method (Figures 3b and S4). The electrical conductivities of hPDI[5] and hPDI[6] are 1 order of magnitude higher than those of shorter ribbons. Such high conductivity is attributed to both the extended ladder conjugation and the array of hydrogen bond donors and acceptors on the primary imide organizing the nanowires.³⁴ The important conclusion is that the electrical conductivity of the hPDI[n] family increases as the ribbons are extended. We estimated the HOMO–LUMO gap of hPDI[n] ribbons from electronic absorption maxima of their alkylated counterpart, hPDI[n]-C11. We used Meier’s method³⁵ to determine the band gap of infinite hPDI[n] polymers to be 1.96 eV, which suggests that hPDI[6] (with a band gap of 2.00 eV) is a good proxy for the polymeric hPDI[n] structures (Figure S2). Therefore, the improvement of electrical conductivity originates from the lengthy conjugated structure of hPDI[n]. Of note, these conductivities are from the undoped molecules, and their anionic forms after reduction presumably have much higher conductivities.³⁶ Taken together, these results show that increasing the length of the conjugated ribbons is an effective way to improve the electrical conductivity.

Electrochemical Performance of hPDI[n]. To evaluate the electrochemical performance of hPDI[n], we prepared the electrodes by drop-casting a slurry of 80 wt % hPDI[n], 10 wt % carbon black (as a conductive agent), and 10 wt % polyvinylidene fluoride (PVDF, as a binder) in *N*-methyl-2-pyrrolidone onto a carbon paper. The carbon paper, which is a common current collector similar to like nickel foam, is used here because of its ability to hold the diluted slurries. Such a high portion of active materials is typical for tests of inorganic

materials but is much higher than those typically tested in organic materials.¹⁸ The electrodes were then assembled with lithium metal and 1 M LiPF_6 in an ethylene carbonate (EC)/diethyl carbonate (DEC) (1:1 by volume) electrolyte in 2032 coin cells. For comparison, we also investigated the PDI monomer and a PDI-vinyl-conjugated polymer (PDIv, section 2.3 of the Supporting Information provides synthetic details) with similar theoretical gravimetric capacities (Figure 3a). The electrochemical impedance spectroscopy (EIS) of these cells reveals that the charge-transfer resistance (R_{ct}) for hPDI[n] decreases as the ribbon is made longer (Figure 3c), PDI exhibits a high R_{ct} of $1400\ \Omega$ (Table S3), and PDIv exhibits similar R_{ct} as hPDI[3]. This trend of R_{ct} correlates well with the electrical conductivity of the pristine materials (Table S3). The low charge-transfer resistance of hPDI[6] ($47\ \Omega$) facilitates fast electron transport, presumably resulting from fast intramolecular and intermolecular charge transfer.

We next performed cyclic voltammetry (CV) to examine the electrochemical behaviors of hPDI[n] ($n = 3-6$), PDI, and PDIv (Figures 3d and S29). At a scan rate of 1 mV/s, hPDI[n] displayed a broad and reversible redox couple at a potential of 2.25 V versus Li/Li^+ , matching the redox events of PDI subunits. The peak current of hPDI[n] increases as the ribbon length increases, revealing the improved electrochemical performance as [n] increases. Analysis on the log-log plot of the sweep rate (ν) versus the peak current (i) shows that hPDI[n] ribbons exhibited surface-controlled kinetics, PDI exhibited diffusion-controlled behavior, and PDIv was in-between (Figure S30). To further demonstrate the contortion effect on lithium-ion transport, we investigate the lithium-ion diffusivity (D_{Li^+}) obtained using EIS (Figure S31 and Table S3).^{37,38} For hPDI[n] series, D_{Li^+} increases as the length of the macro-molecule increases from hPDI[3] ($1.8 \times 10^{-11}\ \text{cm}^2/\text{s}$) to hPDI[6] ($5.7 \times 10^{-10}\ \text{cm}^2/\text{s}$, Table S3). This D_{Li^+} increment as

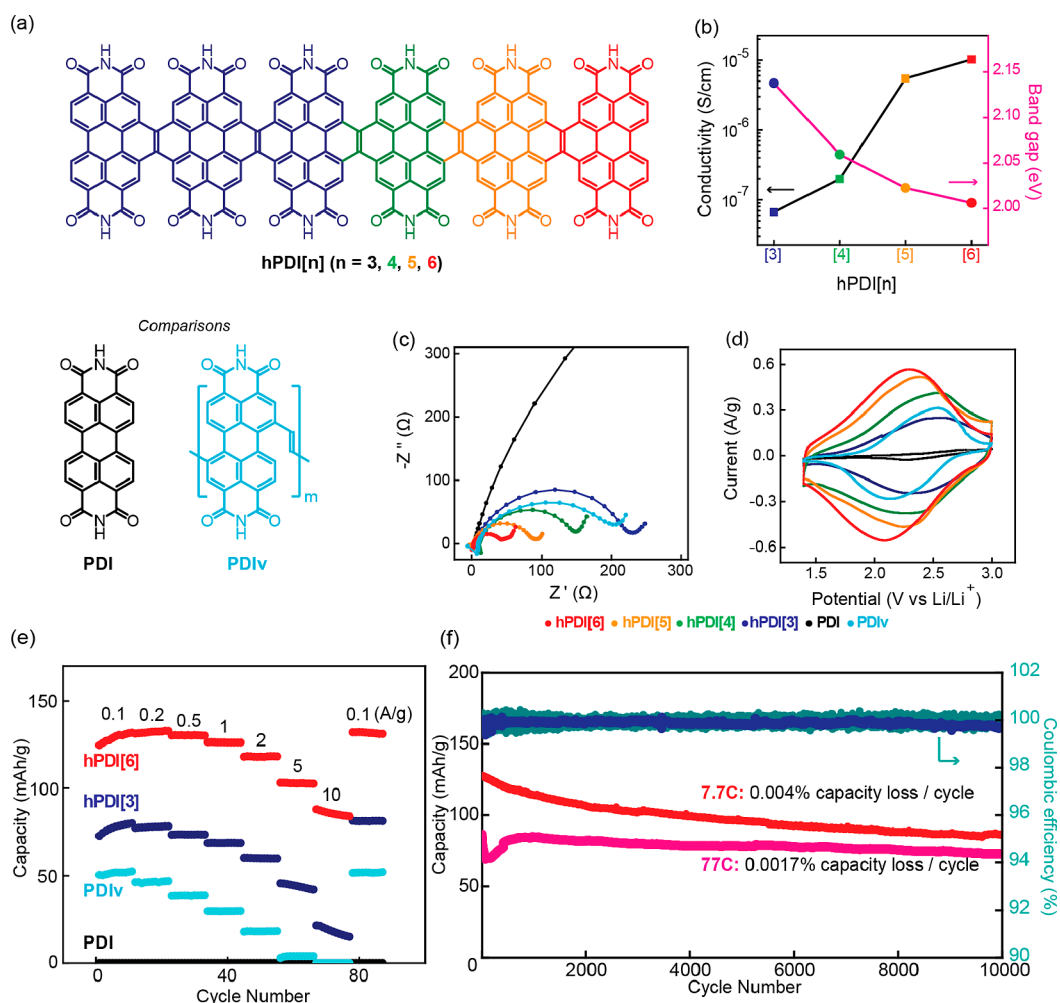


Figure 3. Electrochemical characterization of **hPDI**[*n*]. (a) Molecular structures of the compounds for comparative studies: **hPDI**[3] (blue), **hPDI**[4] (green), **hPDI**[5] (orange), **hPDI**[6] (red), **PDI** (black), and **PDIv** (cyan). (b) Electrical conductivities and band gaps of **hPDI**[*n*]. Band gaps were estimated from the optical energy gaps of **hPDI**[*n*]-C11s. (c) EIS and (d) CV (scan rate: 1 mV/s) of all cathode materials. (e) Rate performance of **PDI**, **PDIv**, **hPDI**[3], and **hPDI**[6]. (f) Cycling performance of **hPDI**[6] at 7.7 C (1 A/g, capacity in red and Coulombic efficiency in cyan) and 77 C (10 A/g, capacity in pink and Coulombic efficiency in blue).

the ribbons extended longer is attributed to both the increase in particle surface area (Figure S6) and the more well-defined contorted carbonyl position. The **PDIv** conjugated polymer, however, exhibited a significantly lower diffusion coefficient of 1.9×10^{-11} cm²/s. Such lower diffusivity of **PDIv** indicates the importance of the well-defined position of the carbonyls imposed by molecular contortion in the longer oligomers.

With significantly improved electrical conductivity and ionic diffusivity, **hPDI**[6] achieved exceptional power density and best-in-class cycling stability as a cathode material. Figure 3e shows the increasing rate capability from **PDI**, **PDIv**, and **hPDI**[3] to **hPDI**[6] at different discharge rates (the rate performance of **hPDI**[4] and **hPDI**[5] can be found in Figure S32). Multiple tests were performed to confirm that the **PDI** monomer had a minuscule capacity at 80% active material mass loading. At 0.1 A/g (0.77 C), **hPDI**[6] had reached 99% of the theoretical specific capacity value (131 mAh/g). It is important to note that **hPDI**[6] exhibited almost no loss in capacity until the rate of the current was increased to 2 A/g. Even at a 100-fold current rate of 10 A/g (77 C), **hPDI**[6] boasted a specific capacity of 87 mAh/g. These results suggest that **hPDI**[6] batteries could be charged to 66% of their capacity within 35 s, corresponding to a specific power density of 22,500 W/kg. We

attribute this exceptional rate performance of **hPDI**[6] to both high ionic diffusivity from the molecular contortion and high electrical conductivity from the precisely defined, “ladder-type” conjugated structure. Recently, Abruña, Fors and co-workers³⁹ have reported an elegant work on phenazine-based OEMs with high energy and power densities by cross-linking, which also demonstrates the effect of increasing conjugation. Importantly, the **hPDI**[6] cathode exhibits extraordinary cycling stability (Figure 3f). At 1 A/g, **hPDI**[6] had an initial capacity of 126 mAh/g and preserved 86 mAh/g after 10,000 cycles at 7.7 C, corresponding to a capacity fade of only 0.004% each cycle. At a higher rate (10 A/g, 77 C), the **hPDI**[6] cathode also maintained its stability, with 84% capacity retention over 10,000 cycles, corresponding to an ultra-low capacity of 0.0017% loss per cycle. Of note, all the **hPDI**[*n*] (*n* = 3–6) cathodes exhibited extraordinary cycling stability (Figure S33). There was a large overpotential from lithium metal, which may have resulted in electrochemical irreversibility and capacity loss when the batteries were operated at a high current density. Even so, these batteries could be cycled for 10,000 cycles with no issue. Collectively, **hPDI**[6] is a very promising fast-charging cathode for its high power density and cycling stability to fill the absence between supercapacitors and batteries.

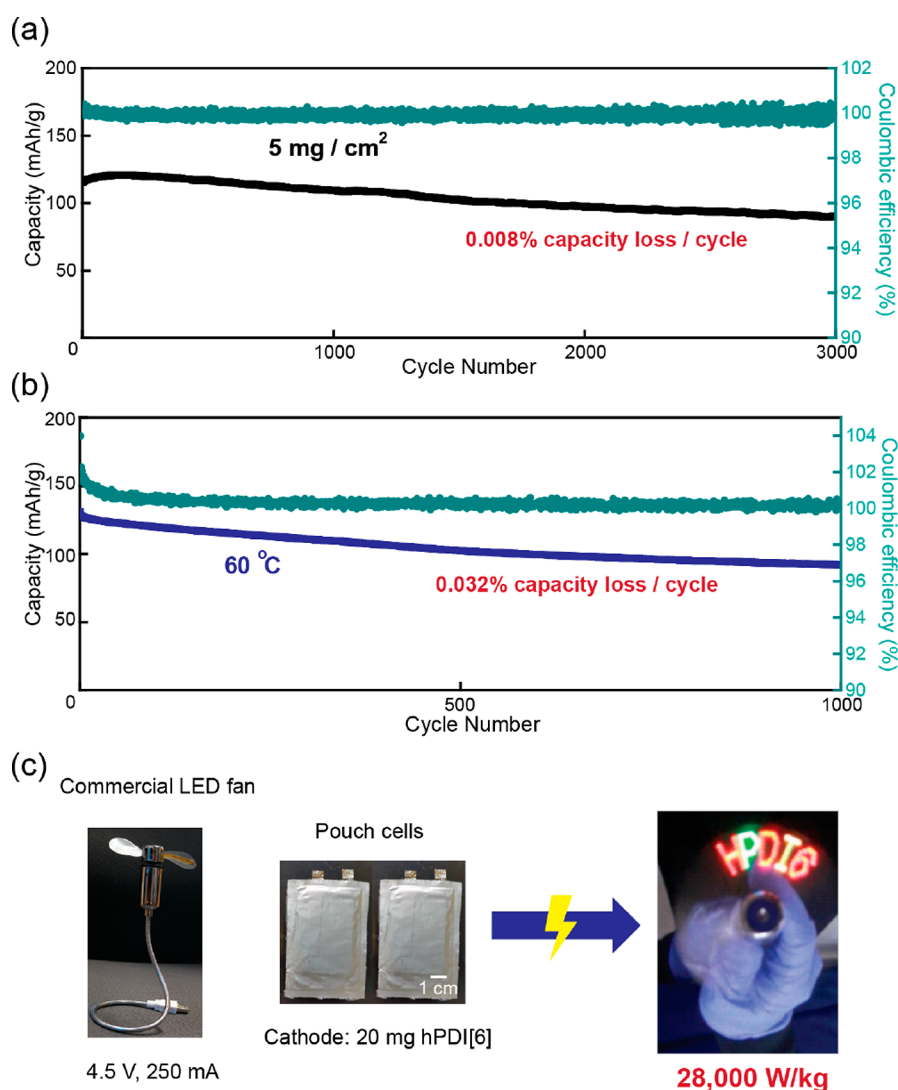


Figure 4. Demonstration of practical application of hPDI[6] batteries. (a) High mass loading of hPDI[6] batteries with an areal mass loading of 5 mg/cm². (b) 60 °C high temperature test. The mass loading was 1 mg/cm². (c) Scheme of hPDI[6] batteries powering an LED fan.

High Mass Loading and High Temperature Test of hPDI[6]. Besides the high rate performance and cycling lifetime, hPDI[6] cathodes were able to maintain their superior performance in both high mass loading and high temperature conditions. To date, most research using organic materials as electrodes are limited to a low mass loading of around 0.1~1 mg/cm² due to materials' low intrinsic electrical conductivity.¹³ To investigate the high active mass loading ability of hPDI[6], we fabricated the electrodes with an active material loading of 5 mg/cm². This material loading is not only a practical mass loading but amongst the highest ever reported in an organic cathode material (Table S1). As shown in Figure 4a, these cells with a high active mass loading were able to maintain 92% of the theoretical specific capacity (121 mAh/g) at 1 A/g and still exhibited high cycling stability with 75% capacity retention after 3,000 cycles. Furthermore, hPDI[6] cathodes also exhibited reliable high temperature performance with an initial capacity of 131 mAh/g and 71% capacity retention after 1000 cycles at 60 °C (Figure 4b).

Practical Demonstration of hPDI[6]. Finally, we demonstrated the practical relevance of hPDI[6] materials by fabricating pouch cells to power a commercial LED fan. The

working voltage and current of the fan were 4–5 V and 200–300 mA, respectively, corresponding to a total power of ~1.12 W. Accordingly, we built pouch cells with an electrode area of 20 cm² and a cathode composite containing 20 mg of hPDI[6]. Two pouch cells were connected in series to provide enough voltage. As shown in Figure 4c and the Supporting Information Video, the battery was able to power the LED fan for 30 s, corresponding to a power density of 28,000 W/kg. Such a power density is 50-fold beyond the current state-of-the-art LIBs. These results show that hPDI[6] can be easily integrated into existing battery-manufacturing processes.

CONCLUSIONS

In summary, we designed and introduced a contorted, atomically defined hPDI[6] macromolecular ladder with high ionic diffusivity and electrical conductivity as a fast-charging and long-lifetime battery cathode. hPDI[*n*] was efficiently synthesized via a newly developed iterative protocol. We found that the electrical conductivity of hPDI[*n*] can be engineered and significantly improved by increasing the conjugation length of the ribbons. In addition, longer hPDI[*n*] ribbons also introduce more contortion sites to accelerate the ion transport. With

improved electrical conductivity and ion diffusivity, hPDI[6] cathodes showed a power density 2 orders of magnitude higher than the conventional inorganic materials. Batteries with hPDI[6] as a cathode can be charged to 66% of their maximum capacity within 35 s. Meanwhile, the stable structure of hPDI[6] allows it to be cycled 10,000 times without significant capacity decay. Moreover, hPDI[6] is also compatible with the existing manufacturing line that can be immediately used for batteries without further modification. These results demonstrate that both the conjugation and contortion are critical to improve the rate performance of organic materials. Such design principles provide a streamlined chemical blueprint for fast charging, long-lifetime, and sustainable battery electrodes.

■ ASSOCIATED CONTENT

SI Supporting Information

The Supporting Information is available free of charge at <https://pubs.acs.org/doi/10.1021/jacs.2c06527>.

Synthetic details and characterization, TGA; UV–vis and FT-IR spectra; conductivity measurement; PXRD; SEM; solution-state NMR spectra; ¹³C solid-state NMR spectra; electrochemical data; and theoretical details (PDF)

hPDI[6] cathode Li battery powering an LED fan (MP4)

■ AUTHOR INFORMATION

Corresponding Authors

Zexin Jin – Department of Chemistry, Columbia University, New York, New York 10027, United States; orcid.org/0000-0002-4971-3656; Email: zj2286@columbia.edu

Yuan Yang – Department of Applied Physics and Applied Mathematics, Columbia University, New York, New York 10027, United States; orcid.org/0000-0003-0264-2640; Email: yy2664@columbia.edu

Colin Nuckolls – Department of Chemistry, Columbia University, New York, New York 10027, United States; orcid.org/0000-0002-0384-5493; Email: cn37@columbia.edu

Authors

Qian Cheng – Department of Chemistry, Columbia University, New York, New York 10027, United States; orcid.org/0000-0001-5510-2977

Si Tong Bao – Department of Chemistry, Columbia University, New York, New York 10027, United States

Ruiwen Zhang – Department of Applied Physics and Applied Mathematics, Columbia University, New York, New York 10027, United States

Austin M. Evans – Department of Chemistry, Columbia University, New York, New York 10027, United States; orcid.org/0000-0002-3597-2454

Fay Ng – Department of Chemistry, Columbia University, New York, New York 10027, United States

Yunhao Xu – Department of Chemistry, Columbia University, New York, New York 10027, United States; orcid.org/0000-0001-6587-9528

Michael L. Steigerwald – Department of Chemistry, Columbia University, New York, New York 10027, United States

Ann E. McDermott – Department of Chemistry, Columbia University, New York, New York 10027, United States; orcid.org/0000-0002-9249-1649

Complete contact information is available at: <https://pubs.acs.org/10.1021/jacs.2c06527>

Author Contributions

[§]Z.J. and Q.C. contributed equally.

Notes

The authors declare no competing financial interest.

■ ACKNOWLEDGMENTS

Primary support for this research was provided by the National Science Foundation under award DMR-2002634. The polymer synthesis was further supported by the U.S. Office of Naval Research under award N00014-20-1-2477. The Columbia University Shared Materials Characterization Laboratory was used extensively for this research. The authors acknowledge the use of instrumentation supported by NSF through the Columbia University, Materials Research Science and Engineering Center under award DMR-2011738. C.N. thanks Sheldon and Dorothea Buckler for their generous support. A.M.E. is supported by the Schmidt Science Fellows, in partnership with the Rhodes Trust. The authors thank Dr. Xiao Xiao and Dr. Cedric Schaack for valuable discussions.

■ REFERENCES

- (1) Goodenough, J. B. How we made the Li-ion rechargeable battery. *Nat. Electron* **2018**, *1*, 204.
- (2) Whittingham, M. S. Lithium Batteries and Cathode Materials. *Chem. Rev.* **2004**, *104*, 4271–4302.
- (3) Yoshino, A. The Birth of the Lithium-Ion Battery. *Angew. Chem., Int. Ed.* **2012**, *51*, 5798–5800.
- (4) Armand, M.; Tarascon, J.-M. Building Better Batteries. *Nature* **2008**, *451*, 652–657.
- (5) Manthiram, A. An Outlook on Lithium Ion Battery Technology. *ACS Cent. Sci.* **2017**, *3*, 1063–1069.
- (6) Goodenough, J. B.; Park, K. S. The Li-Ion Rechargeable Battery: A Perspective. *J. Am. Chem. Soc.* **2013**, *135*, 1167–1176.
- (7) Keyser, M.; Pesaran, A.; Li, Q.; Santhanagopalan, S.; Smith, K.; Wood, E.; Ahmed, S.; Bloom, I.; Dufek, E.; Shirk, M.; Meintz, A.; Kreuzer, C.; Michelbacher, C.; Burnham, A.; Stephens, T.; Francfort, J.; Carlson, B.; Zhang, J.; Vijayagopal, R.; Hardy, K.; Dias, F.; Mohanpurkar, M.; Scofield, D.; Jansen, A. N.; Tanim, T.; Markel, A. Enabling Fast Charging – Battery Thermal Considerations. *J. Power Sources* **2017**, *367*, 228–236.
- (8) Burnham, A.; Dufek, E. J.; Stephens, T.; Francfort, J.; Michelbacher, C.; Carlson, R. B.; Zhang, J.; Vijayagopal, R.; Dias, F.; Mohanpurkar, M.; Scofield, D.; Hardy, K.; Shirk, M.; Hovsapiyan, R.; Ahmed, S.; Bloom, I.; Jansen, A. N.; Keyser, M.; Kreuzer, C.; Markel, A.; Meintz, A.; Pesaran, A.; Tanim, T. R. Enabling Fast Charging – Infrastructure and Economic Considerations. *J. Power Sources* **2017**, *367*, 237–249.
- (9) Ahmed, S.; Bloom, I.; Jansen, A. N.; Tanim, T.; Dufek, E. J.; Pesaran, A.; Burnham, A.; Carlson, R. B.; Dias, F.; Hardy, K.; Keyser, M.; Kreuzer, C.; Markel, A.; Meintz, A.; Michelbacher, C.; Mohanpurkar, M.; Nelson, P. A.; Robertson, D. C.; Scofield, D.; Shirk, M.; Stephens, T.; Vijayagopal, R.; Zhang, J. Enabling Fast Charging – A Battery Technology Gap Assessment. *J. Power Sources* **2017**, *367*, 250–262.
- (10) Liu, Y.; Zhu, Y.; Cui, Y. Challenges and Opportunities towards Fast-Charging Battery Materials. *Nat. Energy* **2019**, *4*, 540–550.
- (11) Augustyn, V.; Come, J.; Lowe, M. A.; Kim, J. W.; Taberna, P. L.; Tolbert, S. H.; Abruña, H. D.; Simon, P.; Dunn, B. High-Rate Electrochemical Energy Storage through Li + Intercalation Pseudocapacitance. *Nat. Mater.* **2013**, *12*, 518–522.
- (12) Yu, Z.; Wang, H.; Kong, X.; Huang, W.; Tsao, Y.; Mackanic, D. G.; Wang, K.; Wang, X.; Huang, W.; Choudhury, S.; Zheng, Y.; Amanchukwu, C. V.; Hung, S. T.; Ma, Y.; Lomeli, E. G.; Qin, J.; Cui, Y.; Bao, Z. Molecular Design for Electrolyte Solvents Enabling Energy-Dense and Long-Cycling Lithium Metal Batteries. *Nat. Energy* **2020**, *5*, 526–533.

- (13) Lu, Y.; Chen, J. Prospects of Organic Electrode Materials for Practical Lithium Batteries. *Nat. Rev. Chem* **2020**, *4*, 127–142.
- (14) Gannett, C. N.; Melecio-Zambrano, L.; Theibault, M. J.; Peterson, B. M.; Fors, B. P.; Abruña, H. D. Organic Electrode Materials for Fast-Rate, High-Power Battery Applications. *Mater. Rep. Energy* **2021**, *1*, 100008.
- (15) Muench, S.; Wild, A.; Friebe, C.; Häupler, B.; Janoschka, T.; Schubert, U. S. Polymer-Based Organic Batteries. *Chem. Rev.* **2016**, *116*, 9438–9484.
- (16) Lee, S.; Kwon, G.; Ku, K.; Yoon, K.; Jung, S.-K.; Lim, H.-D.; Kang, K. Recent Progress in Organic Electrodes for Li and Na Rechargeable Batteries. *Adv. Mater.* **2018**, *30*, 1704682.
- (17) Bhosale, M. E.; Chae, S.; Kim, J. M.; Choi, J. Y. Organic Small Molecules and Polymers as an Electrode Material for Rechargeable Lithium Ion Batteries. *J. Mater. Chem. A* **2018**, *6*, 19885–19911.
- (18) Liang, Y.; Yao, Y. Positioning Organic Electrode Materials in the Battery Landscape. *Joule* **2018**, *2*, 1690–1706.
- (19) Larcher, D.; Tarascon, J. M. Towards Greener and More Sustainable Batteries for Electrical Energy Storage. *Nat. Chem.* **2015**, *7*, 19–29.
- (20) Nishide, H.; Oyaizu, K. Toward Flexible Batteries. *Science* **2008**, *319*, 737–738.
- (21) Poizot, P.; Gaubicher, J.; Renault, S.; Dubois, L.; Liang, Y.; Yao, Y. Opportunities and Challenges for Organic Electrodes in Electrochemical Energy Storage. *Chem. Rev.* **2020**, *120*, 6490–6557.
- (22) Zhong, Y.; Trinh, M. T.; Chen, R.; Wang, W.; Khlyabich, P. P.; Kumar, B.; Xu, Q.; Nam, C.-Y.; Sfeir, M. Y.; Black, C.; Steigerwald, M. L.; Loo, Y.-L.; Xiao, S.; Ng, F.; Zhu, X.-Y.; Nuckolls, C. Efficient Organic Solar Cells with Helical Perylene Diimide Electron Acceptors. *J. Am. Chem. Soc.* **2014**, *136*, 15215–15221.
- (23) Zhong, Y.; Sisto, T. J.; Zhang, B.; Miyata, K.; Zhu, X.-Y.; Steigerwald, M. L.; Ng, F.; Nuckolls, C. Helical Nanoribbons for Ultra-Narrowband Photodetectors. *J. Am. Chem. Soc.* **2017**, *139*, 5644–5647.
- (24) Zhong, Y.; Kumar, B.; Oh, S.; Trinh, M. T.; Wu, Y.; Elbert, K.; Li, P.; Zhu, X.; Xiao, S.; Ng, F.; Steigerwald, M. L.; Nuckolls, C. Helical Ribbons for Molecular Electronics. *J. Am. Chem. Soc.* **2014**, *136*, 8122–8130.
- (25) Peurifoy, S. R.; Castro, E.; Liu, F.; Zhu, X.-Y.; Ng, F.; Jockusch, S.; Steigerwald, M. L.; Echegoyen, L.; Nuckolls, C.; Sisto, T. J. Three-Dimensional Graphene Nanostructures. *J. Am. Chem. Soc.* **2018**, *140*, 9341–9345.
- (26) Castro, E.; Sisto, T. J.; Romero, E. L.; Liu, F.; Peurifoy, S. R.; Wang, J.; Zhu, X.; Nuckolls, C.; Echegoyen, L. Cove-Edge Nanoribbon Materials for Efficient Inverted Halide Perovskite Solar Cells. *Angew. Chem., Int. Ed.* **2017**, *56*, 14648–14652.
- (27) Jin, Z.; Cheng, Q.; Evans, A. M.; Gray, J.; Zhang, R.; Bao, S. T.; Wei, F.; Venkataraman, L.; Yang, Y.; Nuckolls, C. π -Conjugated redox-active two-dimensional polymers as organic cathode materials. *Chem. Sci.* **2022**, *13*, 3533–3538.
- (28) Peurifoy, S. R.; Russell, J. C.; Sisto, T. J.; Yang, Y.; Roy, X.; Nuckolls, C. Designing Three-Dimensional Architectures for High-Performance Electron Accepting Pseudocapacitors. *J. Am. Chem. Soc.* **2018**, *140*, 10960–10964.
- (29) Russell, J. C.; Posey, V. A.; Gray, J.; May, R.; Reed, D. A.; Zhang, H.; Marbella, L. E.; Steigerwald, M. L.; Yang, Y.; Roy, X.; Nuckolls, C.; Peurifoy, S. R. High-Performance Organic Pseudocapacitors via Molecular Contortion. *Nat. Mater.* **2021**, *20*, 1136–1141.
- (30) Bhosale, M. E.; Krishnamoorthy, K. Chemically Reduced Organic Small-Molecule-Based Lithium Battery with Improved Efficiency. *Chem. Mater.* **2015**, *27*, 2121–2126.
- (31) Schuster, N. J.; Hernández Sánchez, R.; Bukharina, D.; Kotov, N. A.; Berova, N.; Ng, F.; Steigerwald, M. L.; Nuckolls, C. A Helicene Nanoribbon with Greatly Amplified Chirality. *J. Am. Chem. Soc.* **2018**, *140*, 6235–6239.
- (32) Li, J.; Ballmer, S. G.; Gillis, E. P.; Fujii, S.; Schmidt, M. J.; Seiko, F. Synthesis of Many Different Types of Organic Small Molecules Using One Automated Process. *Science* **2015**, *347*, 1221–1226.
- (33) Blair, D. J.; Chitti, S.; Trobe, M.; Kostyra, D. M.; Haley, H. M. S.; Hansen, R. L.; Ballmer, S. G.; Woods, T. J.; Wang, W.; Mubayi, V.;

Schmidt, M. J.; Pipal, R. W.; Morehouse, G. F.; Palazzolo Ray, A. M. E.; Gray, D. L.; Gill, A. L.; Burke, M. D. Automated Iterative Csp3–C Bond Formation. *Nature* **2022**, *604*, 92–97.

(34) Wu, J.; Rui, X.; Long, G.; Chen, W.; Yan, Q.; Zhang, Q. Pushing Up Lithium Storage through Nanostructured Polyazaacene Analogues as Anode. *Angew. Chem., Int. Ed.* **2015**, *54*, 7354–7358.

(35) Meier, H.; Stalmach, U.; Kolshorn, H. Effective Conjugation Length and UV/Vis Spectra of Oligomers. *Acta Polym.* **1997**, *48*, 379–384.

(36) Liang, Y.; Chen, Z.; Jing, Y.; Rong, Y.; Facchetti, A.; Yao, Y. Heavily N-Dopable π -Conjugated Redox Polymers with Ultrafast Energy Storage Capability. *J. Am. Chem. Soc.* **2015**, *137*, 4956–4959.

(37) Wang, S.; Wang, Q.; Shao, P.; Han, Y.; Gao, X.; Ma, L.; Yuan, S.; Ma, X.; Zhou, J.; Feng, X.; Wang, B. Exfoliation of Covalent Organic Frameworks into Few-Layer Redox-Active Nanosheets as Cathode Materials for Lithium-Ion Batteries. *J. Am. Chem. Soc.* **2017**, *139*, 4258–4261.

(38) Ho, C.; Raistrick, I. D.; Huggins, R. A. Application of A-C Techniques to the Study of Lithium Diffusion in Tungsten Trioxide Thin Films. *J. Electrochem. Soc.* **1980**, *127*, 343–350.

(39) Gannett, C. N.; Peterson, B. M.; Shen, L.; Seok, J.; Fors, B. P.; Abruña, H. D. Cross-Linking Effects on Performance Metrics of Phenazine-Based Polymer Cathodes. *ChemSusChem* **2020**, *13*, 2428–2435.

Recommended by ACS

Acene-Extended Triptycenes: Synthesis, Characterization, and Singlet Exciton Fission Properties

Yuxiao Duan, Lei Zhang, *et al.*

MARCH 15, 2022
THE JOURNAL OF ORGANIC CHEMISTRY

READ 

Nitrogen-Embedded Quintuple [7]Helicene: A Helicene-Azacorannulene Hybrid with Strong Near-Infrared Fluorescence

Yin-Fu Wu, Lan-Sun Zheng, *et al.*

JUNE 07, 2022
JOURNAL OF THE AMERICAN CHEMICAL SOCIETY

READ 

High-Performance Organic Electronic Materials by Contorting Perylene Diimides

Cedric Schaack, Colin Nuckolls, *et al.*

DECEMBER 23, 2021
JOURNAL OF THE AMERICAN CHEMICAL SOCIETY

READ 

B,N-Embedded Double Hetero[7]helicenes with Strong Chiroptical Responses in the Visible Light Region

Ji-Kun Li, Xiao-Ye Wang, *et al.*

OCTOBER 19, 2021
JOURNAL OF THE AMERICAN CHEMICAL SOCIETY

READ 

Get More Suggestions >